

# 4D Generic Video Object Proposals

Aljoša Ošep, Paul Voigtlaender, Mark Weber, Jonathon Luiten, and Bastian Leibe  
 Computer Vision Group  
 Visual Computing Institute  
 RWTH Aachen University, Germany

{osep, voigtlaender, luiten, leibe}@vision.rwth-aachen.de mark.weber1@rwth-aachen.de

## Abstract

Many high-level video understanding methods require input in the form of object proposals. Currently, such proposals are predominantly generated with the help of networks that were trained for detecting and segmenting a set of known object classes, which limits their applicability to cases where all objects of interest are represented in the training set. This is a restriction for automotive scenarios, where unknown objects can frequently occur. We propose an approach that can reliably extract spatio-temporal object proposals for both known and unknown object categories from stereo video. Our 4D Generic Video Tubes (4D-GVT) method combines motion cues, stereo data, and data-driven object instance segmentation in a probabilistic framework to compute a compact set of video-object proposals that precisely localizes object candidates and their contours in 3D space and time. Our experiments show that on a sequence level, our 4D-GVT can compete with state-of-the-art tracking-by-detection methods on known object classes, while reaching instance segmentation results on the frame level that generalize to unseen classes as well as those of Mask<sup>X</sup> R-CNN, a recent large-scale instance segmentation approach, trained using two orders of magnitude more data.

## 1. Introduction

The main result of this paper is a novel approach for generating high-quality spatio-temporal object tube proposals for both *known* and *unknown* objects from stereo video (Fig. 1). The resulting tube proposals are localized in 3D space and capture the evolution of an object’s visible area over time, *i.e.*, they provide a temporally consistent object segmentation over a video sequence (Fig. 2). Such tube proposals can be useful as basic primitives for a wide variety of applications, ranging from object tracking [73, 5, 27] to action/activity recognition [20], object category discovery [69, 52, 30, 29, 53, 56, 77, 64] and zero-shot learning [78, 72, 50, 2]. 4D stereo-based reconstruction and lo-



Figure 1: We propose a method for generating 4D video-object tube proposals of arbitrary objects from real-world videos and demonstrate generalization to objects of unknown categories (visualized with a red border).

calization in 3D space and time open further possibilities for using 4D-GVT as a building block for learning trajectory prediction [28, 13, 1] and 3D shape completion [74, 57]. These applications are of great importance for automotive applications, in which the capability to perceive and react to unseen dynamic objects is a vital safety concern (see Fig. 1).

Up to now, high-quality object tube proposals could only be generated either by 1) applying a pre-trained object detector for known classes and performing instance segmentation in every frame [15, 55]; or by 2) starting from a manual object mask initialization and applying a video object segmentation approach [67, 22, 4]. The significant contribution of our approach is that it can provide a compact set of high-quality object tubes for multiple objects with automatic initialization, while scaling well to unseen object classes.

This result opens up exciting possibilities for many applications that can take tube proposals as their input. In particular, our approach is efficient enough that it can be applied for video mining in large video collections. We demonstrate its capabilities by applying it for object tube

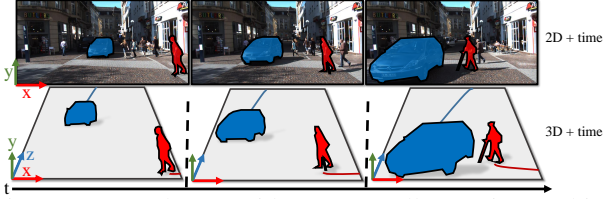


Figure 2: 4D tubes provide a temporally consistent object segmentation in image and 3D space + time.

mining on 14h of driving video (8 million frames) of the Oxford RobotCar dataset [36]. We compare the obtained results on the image level to those of the Mask<sup>X</sup> R-CNN, a large-scale instance segmentation approach by [21] that is trained jointly on COCO [34] and Visual Genome [26] datasets on 3000 classes. Our results show that our approach (4D-GVT) matches accuracy/recall for *known* and *unknown* objects, despite only using knowledge about the 80 COCO classes! In addition, our approach precisely tracks each candidate object in 3D.

The key idea behind our approach is to make use of parallax as a cue to identify temporally consistent object tubes under egomotion of the recording vehicle. We leverage recent developments in object instance segmentation [15] and propose a simple, yet effective probabilistic approach for video proposal generation that combines image instance segmentation, stereo, and sparse scene flow cues. In a nutshell, our proposed 4D-GVT method extends Mask R-CNN [15] to extract frame-level object proposals and their segmentation masks for arbitrary objects. It then localizes these image regions in 3D space and predicts their 3D motion. Taking parallax as a consistency filter, our approach narrows down the potentially vast set of tube continuations to those that are consistent with the object’s perceived relative motion. As a result, 4D-GVT can quickly trim down a large initial set of frame-level region proposals and turn them into a temporally consistent set of object tubes with accurately tracked object positions. Our experiments show that when applying our 4D-GVT proposal generator for car and pedestrian tracking on the KITTI dataset [10], it reaches close to state-of-the-art performance even when compared to dedicated tracking-by-detection methods. We will make all code and data available upon publication.

## 2. Related Work

**Video-Object Mining.** Video-Object mining (VOM) refers to a task of pattern discovery in video collections. It has been used for improving object detectors by mining hard-negatives for specific object categories from web-videos [58, 24], for learning new detectors for objects by localizing mostly single, dominant objects in videos [49] and for tracking-based semi-supervised learning, in which sparse annotations extended by tracks were leveraged in order to extend the amount of training data [37, 38].

The above-mentioned methods have in common that they all need to localize video tubes (or object tracks) from video. Such video tubes or object tracks can be extracted with help of a pre-trained object detector [31, 75]. The drawback of such methods is that they can only localize objects, for which a sufficient amount of training data is available for training object detectors. In realistic driving scenarios, however, it is not feasible to obtain training data for every possible object of interest. For that reason, the most common approach for video-object mining and self-supervised learning in automotive scenarios is based on unsupervised segmentation of 3D sensory data (e.g., LiDAR) using information such as spatial proximity and motion cues [7, 17, 18, 60, 59]. There are a few methods that proposed similar ideas in the vision community by using image-based object proposals as leads for tracking [76, 27, 19], often leveraging stereo information [42, 44, 39, 32] or motion cues [62]. The approach most similar to ours is the category-agnostic multi-object tracker by [44]. It uses two networks, one for proposal generation and one for track classification, in addition to high-quality dense scene flow [65] for data association. In contrast, we propose 1) a unified network that provides per-frame mask-level object proposals and a classification branch and 2) a probabilistic framework for offline video-tube generation, derived from well-established MHT theory [51]. Different to [44], our approach models long-term interactions between the tubes and utilizes the full video sequence for scoring. As a result, our approach generates tubes that are significantly more stable over time, as our results demonstrate.

**Video-Object Segmentation.** Alternatively, object instances can be mined from video using video-object segmentation (VOS), which refers to a task of segmenting objects in videos with weak supervision, typically in the form of pixel masks or bounding boxes: [68, 67, 22, 4]. Such approaches were successfully used in the context of video-based semi-supervised and self-supervised learning [37, 38, 49]. Existing methods for unsupervised video-object segmentation are limited to segmenting a single object of interest (*i.e.* performing object *vs.* background classification) [9, 61, 33, 33]. Both, weakly-supervised and unsupervised VOS methods assume that the object of interest appears from the beginning to the end of the video, with possible short occlusions. This requires a careful video selection and post-processing. In contrast, we assume real-world automotive and robotics scenarios, where such assumptions do not hold. In such scenarios, multiple objects are entering and leaving the field of view frequently.

**Open-set Segmentation.** Many real-world scenarios require reliable segmentation that is not limited to a few categories for which fully labeled training data is available. Mask<sup>X</sup> R-CNN [21] tackles this problem by using partial supervision of bounding boxes to perform instance seg-

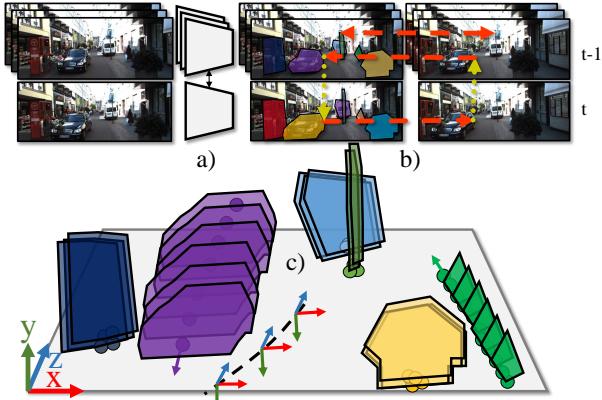


Figure 3: We obtain 4D Video Tubes by a) extracting frame-level object proposals from a video stream using a pre-trained network, b) match features in order to estimate depth and sparse scene flow to localize proposals in 3D and estimate their velocity and finally, c) associate these 3D segments to obtain a set of video tubes.

mentation for the Visual Genome dataset that includes labels for over 3000 categories. Pham *et al.* [46] address the problem of open-set segmentation by fusing modern instance segmentation with traditional unsupervised methods to obtain instance segmentation for an unbounded number of categories. In contrast, our model leverages its in-built category-agnostic detection to generalize to objects of *unknown* categories on a video-level.

**Possible Applications.** Our 4D-GVTs are a flexible tool that can be used for many different applications. A particularly interesting application for object proposals is the automatic discovery of new object categories [52, 30, 29, 53, 56, 77, 40, 64], a task related to zero-shot learning [78, 72, 50, 2]. Video-based object discovery has so far been addressed using weak [69], semantic [63] or no supervision [49, 27]. However, most current methods are limited to only simple scenarios containing a single or only a few objects of interest. In contrast, our approach addresses real-world scenarios, captured from mobile platforms, in which several objects per image typically occur. Due to precise stereo-based localization and reconstruction of tubes, we believe our video proposals can be used as training data for tasks such as trajectory clustering, prediction and abnormality detection [28, 13, 25, 1, 35] and for learning 3D shape-completion [74, 57]. With those applications in mind we have created a dataset of 4D-GVT video tubes for 14h of driving video that we will make available upon publication.

### 3. Method

We first provide a brief outline of our approach and then introduce its steps in detail. From each video-frame of the video sequence, we extract image-level object proposals (Fig. 3a), defined by an object pixel mask. Next, we

localize these mask proposals in 3D camera space and predict their motion by computing sparse scene flow, obtained by matching image features (Fig. 3b). Using the estimated depth and pixel mask, we localize these proposals in 3D space and associate them in space-time in order to obtain a set of 4D Video Proposal Tubes (Fig. 3c). We derive a probabilistic model from well-established MHT theory [51] that fuses objectness score provided by the proposal network together with motion and temporal mask consistency cues and that performs an additional inference step that suppresses tubes with significant overlap in space-time. This way, we combine a learning-based method for generic instance segmentation with a powerful prior knowledge about motion/shape consistency and scene geometry in a sound probabilistic framework. In the following, we provide a detailed outline of each step of our method.

#### 3.1. Image-Level Proposals with MP R-CNN

First, we need to obtain cues for potential objects on the video-frame level. As we do not want to limit ourselves to obtaining image-level cues only for the most common object categories for which we can obtain a sufficient amount of training data (*e.g.* using Mask R-CNN [15]), we propose a category-agnostic variant of Mask R-CNN, Mask Proposal R-CNN (MP R-CNN), whose classification part only disambiguates objects from the background. We achieve that by first training the network in the category-agnostic setting, *i.e.* by merging all 80 COCO classes into one “object” class. By only distinguishing between objects and non-objects, we expect a better generalization to object categories that are either not present or not annotated in COCO. We confirm experimentally in Sec. 4 that this procedure indeed generalizes to unseen object classes (*i.e.*, classes that were held-out during the training). In order to retain a capability to perform higher-granularity classification for objects that appeared in the training set, we add a second classification head (identical to the normal classification head of Mask R-CNN) to this network which disambiguates between the 80 classes. At test time, the category-agnostic classification head is used to provide confidence scores for proposals, and the second classification head is additionally evaluated to provide a posterior distribution over the 80 classes for each proposal. By thresholding the confidence of the class-specific classification head, we can again divide the proposals into a class-specific and a class-agnostic set. By adding the category-specific head, we thus retain class information when it is available and achieve a performance comparable to the class-specific version, while still retaining a good generalization ability to unseen classes due to the category-agnostic head as our experiments demonstrate.

### 3.2. 4D Video Tubes

To get from image-level proposals to 4D Video Tubes, we combine modern instance segmentation methods, trained in a category-agnostic setting, with well-understood tracking theory [31, 51]. Formally, we obtain a set of frame-level object proposals  $\mathcal{P}^{0:T}$  in the frame-range  $0 \rightarrow T$ ,  $\mathcal{P}^t = \{\mathcal{S}_j^t, t \in 0 \dots T\}$  from MP R-CNN. The  $j$ -th per-frame proposal is defined as  $\mathcal{S}_j^t = [\mathbf{p}_j^t, \mathbf{v}_j^t, \mathbf{s}_j^t, \mathbf{c}_j^t, \mathbf{m}_j^t, \mathbf{s}_j^t]$ . The mask  $\mathbf{m} \in \{0, 1\}^{w \times h}$  for an image of size  $w \times h$ , objectness score  $s \in [0, 1]$  and category information  $\mathbf{c} \in \mathbb{R}^{81}$  (i.e. one of *known* 80 COCO classes or *unknown*) are obtained by the MP R-CNN network.

This information is extended by 3D position  $\mathbf{p} \in \mathbb{R}^3$ , 3D size  $\mathbf{s} \in \mathbb{R}^3$  and velocity vector  $\mathbf{v} \in \mathbb{R}^3$  from the video sequence as follows. For each video sequence, we match local Harris corner based image features of 1) left-right images coming from stereo and 2) forward-backward in time for two consecutive neighboring frames  $(t-1) \rightarrow t$ . Features that pass a cyclic consistency check (left, right, forward, backward) are used to estimate sparse scene flow. We triangulate left-right matches in two consecutive frames and compute difference vectors  $((t-1) \rightarrow t)$  for all successful matches. Using the same set of feature matches, we obtain an egomotion estimate  $E^{(t-1) \rightarrow t}$  by minimizing the re-projection error using non-linear least squares [12] and we finally keep left-right image matches to obtain a scene depth estimate  $D^t$  using the feature-matching based method of [11]. By cropping stereo and scene flow estimates within the estimated mask area, we robustly compute the 3D position, velocity and 3D bounding box for each proposal.

**Video Tube Proposals** After obtaining a set of per-frame object proposals  $\mathcal{P}^{0:T}$  for a video sequence that spans from frame  $0 \rightarrow T$ , we partition these into a 4D tube proposal set, i.e., a set of video tube proposals  $\mathcal{A}^{0:T} = \{\mathcal{T}_i^{n:m}\}$ , where each tube proposal  $\mathcal{T}_i$  spans over a frame range of  $n$  to  $m$ .

Obtaining such partitions is a very challenging, multi-dimensional assignment problem: object proposals may originate from objects, as well as from segmentation clutter. Obtaining an exact solution to multi-frame assignment problems in tracking is NP-hard, and we need to resort to approximate solutions. One possibility would be to use an approach like MHT [51], which maintains a tree of potential associations for each possible object and to perform tree pruning in order to avoid combinatorial explosion. However, for a large number of per-frame object proposals, maintaining such a tree would be prohibitively expensive.

Instead, we resort to the forward-backward track enumeration algorithm [31], guided by the estimated scene flow. We perform a forward-backward data association by sliding a temporal window over the whole video sequence. For each video frame  $t$ ,  $t \in 0 \dots T$ , we 1) extend the existing tube proposal set using  $\mathcal{P}^t$  and 2) attempt to start a new

object tube from each unassigned proposal by performing bi-directional data association within a temporal window.

In order to minimize incorrect associations, which would lead to spurious tubes, we leverage object motion models, the rigidity of the 3D scene, and the known image formation model to guide frame-to-frame proposal data association to only a small set of feasible associations. This is done as follows (similar to [44]). Using an estimate of frame-level object proposals with 3D position  $\mathbf{p}$ , velocity  $\mathbf{v}$  and size  $\mathbf{s}$  from each frame-level proposal, we start a new tube and estimate its state recursively using a linear Kalman filter. We perform association in the following steps. First, we perform a Kalman filter prediction in order to estimate a 3D position and perform 3D position based gating in order to severely narrow down the set of feasible proposal associations. Then we predict the segmentation mask of the object in the current frame, and finally we extend the tube with the proposal that maximizes joint association probability based on mask IoU (image domain) and 3D position.

We obtain the mask prediction  $\tilde{\mathbf{m}}_i^t \in \{0, 1\}^{w \times h}$  of tube  $\mathcal{T}_i$  for video-frame  $t \in 1 \dots T$  based on a 2D mask estimate of the last associated mask  $\mathbf{m}_i^{(t-1)}$ , the depth  $D^t$  and egomotion estimate  $E^{(t-1) \rightarrow t}$ :

$$\mathcal{J} = \pi(K E^{(t-1) \rightarrow t} M_i^{(t-1) \rightarrow t} K^{-1} \pi^{-1}(\mathbf{m}_i^{(t-1)} \odot D^{(t-1)})),$$

$$\tilde{\mathbf{m}}_i^t(\mathbf{p}') = \begin{cases} 1, & \mathbf{p}' \in \mathcal{J} \\ 0, & \text{else} \end{cases}, \quad (1)$$

where  $\pi : \mathbb{R}^3 \rightarrow \mathbb{R}^2$  and  $\pi^{-1} : \mathbb{R}^2 \rightarrow \mathbb{R}^3$  denotes the camera projection/backprojection operator (applied element-wise),  $K$  denotes the known camera matrix and  $\odot$  performs element-wise multiplication. The matrix  $M_i^{(t-1) \rightarrow t}$  represents estimated motion of the tube by the Kalman filter. Thus, starting from the per-frame proposals  $\mathcal{P}^{0:T}$  over the video sequence, obtained from the MP R-CNN network and localized in 3D space, we have now linked these proposal segments together into a set of proposal video tubes  $\mathcal{A}^{0:T}$ .

**Scoring Tube Proposals.** Following MHT theory, [51], we obtain a ranked set of relevant video tube proposals by scoring tubes using log-likelihood ratios between the proposal tube and the null hypothesis tube. The null tube encodes tubes generated from random background clutter. The score  $\theta(\cdot)$  of the tube  $\mathcal{T}_i$  is a linear combination of the tube motion score, the mask consistency score and the tube objectness score (we are omitting time indices for brevity):

$$\theta(\mathcal{T}_i) = w_1 \cdot \vartheta_{\text{mot}}(\mathcal{T}_i) + w_2 \cdot \vartheta_{\text{mask}}(\mathcal{T}_i) + w_3 \cdot \vartheta_{\text{obj}}(\mathcal{T}_i). \quad (2)$$

Intuitively, the **tube motion score** encodes the assumption that objects move smoothly. It takes the form of a likelihood ratio test, comparing the probability that the tube corresponds to a valid object tube to the null hypothesis that the tube was generated from random background clutter:

$$\vartheta_{\text{mot}}(\mathcal{T}_i^{n:m}) = \ln \frac{p(\mathbf{p}_{\mathcal{T}_i}^{n:m} | \mathcal{I}_i \subseteq \mathcal{T}_i^{n:m})}{p(\mathbf{p}_{\mathcal{T}_i}^{n:m} | \mathcal{I}_i \subseteq \mathcal{T}_\emptyset)}. \quad (3)$$

The notation  $\mathcal{I}_i \subseteq \mathcal{T}_i^{n:m}$  denotes that the 3D position observations originate from the tube  $\mathcal{T}_i^{n:m}$  and  $\mathcal{T}_\emptyset$  denotes the null tube hypothesis. The set  $\mathcal{I}_i^{n:m} = \{\mathcal{S}_{k_i}^t \mid n \leq t \leq m\}$  denotes the supporting image-level proposal set of a tube, where  $k_i$  refers to the  $k$ -th frame-level proposal that supports  $\mathcal{T}_i$  at a certain frame  $t$ . The Markovian motion assumption and conditional independence assumption of the observations originating from the null tube hypothesis lead to the following factorization of Eq. 3:

$$\begin{aligned} p(\mathbf{p}_{\mathcal{I}_i}^{n:m} \mid \mathcal{I}_i \subseteq \mathcal{T}_i^{n:m}) &= \prod_{t=n}^m p(\mathbf{p}^t \mid \mathbf{p}_{\mathcal{I}_i}^{(n-1):(t-1)}, \mathcal{I}_i \subseteq \mathcal{T}_i^{n:t}) \\ &= \prod_{t=n}^m \mathcal{N}(\mathbf{p}^t; \tilde{\mathbf{p}}^t, \tilde{\Sigma}^t), \end{aligned} \quad (4)$$

$$p(\mathbf{p}_{\mathcal{I}_i}^{n:m} \mid \mathcal{I}_i \subseteq \mathcal{T}_\emptyset) = \prod_{t=n}^m p(\mathbf{p}_{\mathcal{I}_i}^t \mid \mathcal{I}_i \subseteq \mathcal{T}_i) = \prod_{t=n}^m \frac{1}{A_{GP}}. \quad (5)$$

The likelihood that the observation originates from the tube is assumed to be Gaussian and is evaluated using the Kalman filter prediction. It measures how well the ground position of an object proposal corresponds to the Kalman filter prediction  $\tilde{\mathbf{p}}^t$  under the estimated variance  $\tilde{\Sigma}^t$  at time  $t$ . This is evaluated against the null hypothesis of a uniform distribution of clutter objects over the sensing area  $A_{GP}$  (roughly  $80m \times 50m$  of the ground plane, estimated from the 3D point cloud).

The **tube mask consistency score** encodes the intuition that the silhouette and position of the object in the image plane do not change significantly on a frame-to-frame level. Again, a likelihood ratio test is used, comparing the mask IoU against a null hypothesis model of no intersection:

$$\vartheta_{\text{mask}}(\mathcal{T}_i^{n:m}) = \ln \frac{p(\mathbf{m}_{\mathcal{I}_i}^{n:m} \mid \mathcal{I}_i \subseteq \mathcal{T}_i^{n:m})}{p(\mathbf{m}_{\mathcal{I}_i}^{n:m} \mid \mathcal{I}_i \subseteq \mathcal{T}_\emptyset)}, \quad (6)$$

following the same assumption as for (3), (6) factorizes as:

$$\begin{aligned} p(\mathbf{m}_{\mathcal{I}_i}^{n:m} \mid \mathcal{I}_i \subseteq \mathcal{T}_i^{n:m}) &= \prod_{t=n}^m p(\mathbf{m}^t \mid \mathbf{m}_{\mathcal{I}_i}^{(n-1):(t-1)}, \mathcal{I}_i \subseteq \mathcal{T}_i^{n:t}) \\ &= \prod_{t=n}^m \text{IoU}(\tilde{\mathbf{m}}^t, \mathbf{m}^t) \end{aligned} \quad (7)$$

$$p(\mathbf{m}_{\mathcal{I}_i}^{n:m} \mid \mathcal{I}_i \subseteq \mathcal{T}_\emptyset) = \prod_{t=n}^m p(\mathbf{m}_{\mathcal{I}_i}^t \mid \mathcal{I}_i \subseteq \mathcal{T}_\emptyset) = \prod_{t=n}^m \frac{1}{\alpha}, \quad (8)$$

Here, we compute frame-to-frame mask consistency as mask intersection-over-union between the mask prediction  $\tilde{\mathbf{m}}^t$  and the (mask) observation  $\mathbf{m}^t$ . The null hypothesis model is a confidence threshold (base value  $\alpha$ ), obtained by hyperparameter optimization.

Finally, the **tube objectness score** utilizes the objectness scores estimated by the network and integrates them over the whole tube:

$$\vartheta_{\text{obj}}(\mathcal{T}_i^{n:m}) = \ln \frac{p(\mathbf{s}_{\mathcal{I}_i}^{n:m} \mid \mathcal{I}_i \subseteq \mathcal{T}_i^{n:m})}{p(\mathbf{s}_{\mathcal{I}_i}^{n:m} \mid \mathcal{I}_i \subseteq \mathcal{T}_\emptyset)}, \quad (9)$$

$$p(\mathbf{s}_{\mathcal{I}_i}^{n:m} \mid \mathcal{I}_i \subseteq \mathcal{T}_i^{n:m}) = \prod_{t=n}^m p(\mathbf{s}_{\mathcal{I}_i}^t \mid \mathcal{I}_i \subseteq \mathcal{T}_i^{n:t}) = \prod_{t=n}^m s^t, \quad (10)$$

$$p(\mathbf{s}_{\mathcal{I}_i}^{n:m} \mid \mathcal{I}_i \subseteq \mathcal{T}_\emptyset) = \prod_{t=n}^m p(\mathbf{s}_{\mathcal{I}_i}^t \mid \mathcal{I}_i \subseteq \mathcal{T}_\emptyset) = \prod_{t=n}^m \frac{1}{\beta}. \quad (11)$$

Here, the likelihood ratio test compares the probability of the tube being a valid object (individual probabilities are estimated by the MP R-CNN network) against a null hypothesis model of the tube belonging to segmentation clutter. The confidence threshold  $\beta$  is a model parameter.

Experimentally, we can observe (Sec. 4) that for *known* object categories, objectness scores extracted from a pre-trained variant of Mask R-CNN [15] provide a great ranking cue. However, for objects that were not in the training set, scores based on temporal mask and motion consistency lead to a significantly better ranking and provide better generalization for objects categories that were not seen during training, *i.e.* that are not in the COCO category set. This observation confirms that all three terms of (2) are necessary.

**Proposal Tubes Co-Selection.** These proposal tubes may still overlap with each other and provide competing explanations for the same image pixels. In order to obtain a compact video tube set, we perform an additional video tube co-selection step that suppresses highly-overlapping tubes. The co-selection is performed by computing a MAP estimate using a CRF model by minimizing the following non-submodular function within batches of 100 frames:

$$F(\mathbf{b}, \mathcal{A}^{n:m}) = \sum_{\mathcal{T}_i \in \mathcal{A}^{n:m}} b_i (\epsilon_1 - \theta(\mathcal{T}_i)) + \epsilon_2 \cdot \sum_{\mathcal{T}_i, \mathcal{T}_j \in \mathcal{A}^{n:m}} b_i b_j \varphi(\mathcal{T}_i, \mathcal{T}_j) \quad (12)$$

$\mathbf{b} \in \{0, 1\}^{|\mathcal{A}^{n:m}|}$  is a binary vector whose elements  $b_i$  indicate that the  $i^{\text{th}}$  tube is selected. The unary term  $\theta(\cdot)$  corresponds to the tube scoring function. The pairwise term  $\varphi(\mathcal{T}_i, \mathcal{T}_j) = \sum_{t=n}^m \ln(\text{IoU}(\mathbf{m}_i^t, \mathbf{m}_j^t))$  integrates image-level temporal mask IoU within the batch and gives a penalty to overlapping tubes. Here,  $\mathbf{m}_i^t$  and  $\mathbf{m}_j^t$  are object masks of tubes  $\mathcal{T}_i$  and  $\mathcal{T}_j$  at frame  $t$ , respectively. The model parameters  $\epsilon_1$  and  $\epsilon_2$  are learned on a held-out validation set of the KITTI dataset [10] using random search.

The presented co-selection reduces the set of video-object tube proposals, such that starting from the unlabelled images of a video sequence, we end up with a compact set of 4D Video Tubes for *known* and *unknown* object categories. Using this formulation, co-selection of tubes in which one tube represents an object and a second one a part of the same object is still possible. For our application, this is desired, because it is not trivial to separate objects and their parts in general. To minimize the energy function (12), we use the multi-branch algorithm by [54].

## 4. Experimental Evaluation

**Datasets.** We evaluate the proposed method on three datasets: COCO [34], Oxford RobotCar [36] and

Category	Car	Person	Bike	Bus	Other	All
#instances	599	354	78	50	413	1494
Portion	40.1%	23.1%	5.2%	3.3%	27.6%	100%

Table 1: We labeled a subset of the Oxford RobotCar dataset for evaluation purpose. We annotated 150 images belonging to different video sequences.

KITTI [10]. On COCO, we evaluate generalization capabilities of our MP R-CNN network. The KITTI dataset is a standard object detection and tracking benchmark in automotive scenarios, captured from a mobile platform equipped with a stereo camera setup. We use the KITTI Multi-Object Tracking benchmark with the *car* and *pedestrian* categories for a sequence-level evaluation of our video tubes.

The Oxford RobotCar dataset was recorded from a car and covers a wide range of different seasons and lighting conditions. The dataset provides a large amount of recorded data (roughly 30h) and covers a broad set of object classes. However, there are no object class labels available. For evaluation purposes, we labeled a subset of the video sequences (see Tab. 1) in order to measure the performance of our method on *known* and *unknown* object classes.

**MP R-CNN Generalization to Unseen Classes.** On the COCO [34] dataset, we follow the standard evaluation protocol and evaluate our model with the average recall (AR) metric for a fixed number of proposals using the minimal split. We show that our proposed method achieves a high AR with only a few proposals per frame and that it is capable of generalizing to *unknown* object categories. We follow the generalization experiment of DeepMask [47] and train the model using a subset of 20 categories that intersect with Pascal VOC [8]. We evaluate the generalization of our model against DeepMask [47], as the follow-up SharpMask paper [48] does not provide generalization experiments. We report the numbers obtained by [47].

Table 5 outlines results obtained by training our (MP R-CNN20) model and the baseline (DeepMask20) on a 20-category subset and evaluating on the full COCO 80 category validation set. Our model performs and generalizes better than the DeepMask baseline. In particular, we achieve 0.261 AR (+0.122) compared to the baseline for top-10 box proposals. Remarkably, our model also performs better than the DeepMask20\* variant (0.152 AR), which uses the fully-trained model for ranking the proposals. Our full model (MP R-CNN80) achieves 0.421 AR (+0.16 AR from the 20-category model). Table 4 highlights the difference between AR obtained on the *known* 20-category set and the full *unknown* 60-category set. As expected, the total recall (AR @ 1000) is lower for the *unknown* category set and we observe a loss in ranking capability. However, MP R-CNN is capable of proposing and segmenting object categories that do not appear in the train-

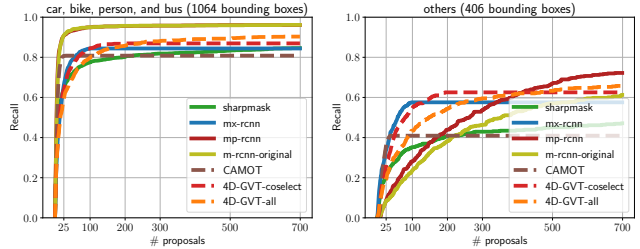


Figure 4: Image-level (solid) and video tube (dashed) proposal and recall evaluation on Oxford. Remark: (■) and (■) follow the same curve in the left plot.

ing set and hence, is suitable for our task. It is not surprising that MP R-CNN outperforms DeepMask, given that it is based on a stronger instance segmentation method [15]. The purpose of this experiment is to demonstrate that MP R-CNN generalizes just as well or better compared to well-established object proposal generators.

**Evaluation on Oxford.** To demonstrate the cross-domain transfer capabilities of MP R-CNN and 4D-GVT, we labeled a small subset of the Oxford RobotCar dataset (see the summary in Tab. 1). Using this set, we compare MP R-CNN and 4D-GVT to several baselines. All methods were trained on the COCO dataset, except Mask<sup>X</sup> R-CNN [21], which was trained on both COCO and Visual Genome [26] with 3000 object categories. Fig. 4 shows recall (at > 0.5 IoU) as a function of the number of object proposals for *known* object categories (intersecting with COCO category set, *left*) and *unknown* object classes (*right*). For image-level evaluation (solid lines), we compare our MP R-CNN (■) to SharpMask [48] (DeepMask successor, ■), Mask<sup>X</sup> R-CNN (■) and standard Mask R-CNN (■) where we merely keep the low-confidence predictions, which is a strong baseline as shown in [46]. As can be seen in Fig. 4 (*left*), our MP R-CNN model (■) and Mask R-CNN (■) perform well on *known* object categories while SharpMask (■) and Mask<sup>X</sup> R-CNN (■) achieve lower recall. On *unknown* object categories Mask<sup>X</sup> R-CNN performs significantly better for top-100 proposals per frame and provides a better ranking, which is not surprising, as it was trained on a large dataset, containing 3000 classes. In a limit for 700 proposals per frame, MP R-CNN (■) and Mask R-CNN (■) achieve higher recall (0.75 and 0.61, respectively) than Mask<sup>X</sup> R-CNN (■) (0.59).

We evaluate our 4D-GVT tubes (dashed lines) on the Oxford RobotCar dataset by extracting video tubes in a 100-frame temporal neighborhood of the 150 labeled images. We show the results obtained using the full tube set (■ ■) and the set obtained after the co-selection step (■ ■), as explained in Sec. 3.2. For *known* classes, we achieve comparable recall to Mask<sup>X</sup> R-CNN (■) with both 4D-GVT variants (■ ■, ■ ■) in the top-100 proposals regime.

For *unknown* categories, Mask<sup>X</sup> R-CNN (■) and both 4D-GVT variants provide an excellent ranking for top-100

Model	AR @ 10	AR @ 100	AR @ 1000
DeepMask20	0.139	0.286	0.431
DeepMask20*	0.152	0.306	0.432
MP R-CNN20	0.261	0.412	0.517
MP R-CNN	0.421	0.608	0.662

(a) Following the evaluation protocol of DeepMask [47], we show the generalization capabilities of our proposal generator on image-level by training on 20 COCO categories and evaluating on all 80 COCO categories.

Table 2: MP R-CNN generalization (Average Recall - AR) to unseen classes on COCO dataset [34].

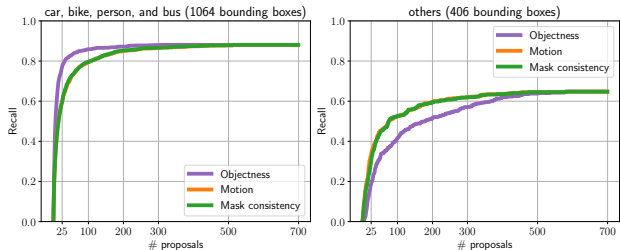


Figure 5: Tube scoring evaluation (Oxford).

proposals. Remarkably, our 4D-GVT proposals achieve same recall and, most importantly, ranking capabilities as Mask<sup>X</sup> R-CNN despite being trained only on the 80 COCO categories. Also supremely important: 4D-GVT tracks the objects and assigns temporarily consistent objects ids, which Mask<sup>X</sup> R-CNN cannot do. This clearly demonstrates that the generalization of Mask R-CNN baseline to *unknown* object classes can be significantly improved by leveraging parallax as consistency filter and motion cues.

A comparison to unsupervised video-object segmentation methods such as [9, 61, 33, 33] is not possible as these methods extract only a single dominant tube, while the sequences from Oxford RobotCar contain several object instances in every video-frame. However, as an additional video-level baseline, we adapt the official implementation of CAMOT [44] and replace the two-stage proposal generation and track classification with our MP R-CNN for fair comparison. As can be seen from 4 (left) CAMOT (■ ■) can track several *unknown* objects, but achieves significantly lower recall (0.4 vs. 0.61 for 4D-GVT -coselect).

Fig. 7 compares the output of (a) our method, (b) Mask<sup>X</sup> R-CNN and (c) Mask R-CNN qualitatively. As can be seen, Mask R-CNN works very well for the 80 classes (*car, bike, person, etc.*). 4D-GVT and Mask<sup>X</sup> R-CNN both segment a large variety of objects. However, only our method additionally provides temporal continuity.

**Scoring Ablation.** We experimentally justify the design decisions for tube scoring (Oxford) in Fig. 5. Clearly, for *known* object categories, tube ranking based on the proposal confidence scores (**objectness**) obtained by MP R-CNN is a strong cue (Fig. 5, left). However, for *unknown* categories (Fig. 5, right), the scoring based on the **mask consistency** and the **motion** scores provide significantly stronger scoring

Evaluation Criteria	AR @ 10	AR @ 100	AR @ 1000
Known COCO Cat. (20)	0.421	0.587	0.641
Unknown COCO Cat. (60)	0.069	0.179	0.338

(b) We evaluate our per-frame proposal generator on *known* and *unknown* categories separately and show that the MP R-CNN is able to generalize to unseen object categories given a sufficient number of proposals, while it performs very well on seen object categories. Since the ground-truth is different (*known* and *unknown*), the numbers are not directly comparable, but the trend is clear.

cues. This further confirms the efficacy of utilizing prior knowledge about motion and temporal shape consistency to compensate for the lack of training data.

**Sequence-Level Evaluation.** We demonstrate sequence-level performance by evaluating our method on our custom split of the training set (details in the supplementary). We follow the official evaluation protocol that evaluates tracking performance using CLEAR-MOT [3] metrics on *car* and *pedestrian* categories, as only these categories are observed frequently enough so that a tracking evaluation is statistically meaningful. In general, we do not know the object categories of the tubes. However, we can use the information obtained from the second (category-specific) classification head (as explained in Sec. 3.1) and obtain the conditional probability for a tube representing a *car* or *pedestrian*, given that it represents an object. We compare our method to the tracking-by-detection approach by [43] (CIWT), which is among the top-4 performers on the KITTI MOT benchmark (comparing methods using public detections, Regionlets [70]) and which thus provides a strong object tracking baseline. This method is tuned for tracking *car* and *pedestrian* categories only and uses dedicated motion models for those categories. In addition, we compare to a stereo-based category-agnostic tracker (CAMOT) [44] that is capable of tracking a large variety of objects. To make the comparison fair, we use the same inputs from MP R-CNN, which is trained on COCO, for CAMOT and our method. In this case, we map COCO category *person* to *pedestrian*. As an additional experiment, we fine-tune MP R-CNN on the KITTI dataset on *car* and *pedestrian* categories, which we can use to evaluate CIWT. Both CAMOT and 4D-GVT output bounding boxes derived from the tracked segment, whereas KITTI MOT assumes amodal bounding boxes.

Table 3 outlines the tracking results for the *car* and *pedestrian* categories. We focus on the MOTA metric and the number of ID switches. We provide the full table with more evaluation metrics in the supplementary material. CIWT achieves the highest MOTA score (0.65) on the *car* category when fine-tuned on KITTI, and our 4D-GVT takes the second place (0.61). This is due to the higher CIWT recall and that our method can only propose tubes in the near camera range (up to 40 – 50m), whereas CIWT can also

	Pedestrian		Car	
	MOTA	IDS	MOTA	IDS
CIWT (KITTI)	<b>0.33</b>	42	<b>0.65</b>	8
CAMOT (KITTI)	0.26	72	0.60	40
4D-GVT (KITTI)	<b>0.33</b>	<b>18</b>	0.61	<b>6</b>
CAMOT (COCO)	-0.05	214	0.54	174
4D-GVT (COCO)	<b>0.27</b>	<b>24</b>	<b>0.57</b>	<b>4</b>

Table 3: Tracking evaluation on KITTI MOT dataset for the *pedestrian* (left) and *car* (right) category.

track in farther ranges in the absence of stereo, as shown in Fig. 6. For the *pedestrian* category, our method and CIWT both achieve 0.33 MOTA, as KITTI pedestrians mainly appear in the near-range. The proposed 4D-GVT consistently outperforms CAMOT in terms of MOTA. As expected, the fine-tuned variants perform better in terms of MOTA score, however, the generic (COCO) model yields better recall in farther camera ranges. These experiments demonstrate that our video-object proposal generator performs better than a state-of-the-art category-agnostic tracker and can compete with top-performing tracking-by-detection methods for *known* object categories. Importantly, our 4D-GVT drastically reduces ID switches, which is very important for video object proposals. It is desirable to extract long video tubes from videos rather than only short fragments. Comparing the fine-tuned model, 4D-GVT commits 18 and 6 ID switches for *car* and *pedestrian*, respectively, compared to 42 and 8 (CIWT); 72 and 40 (CAMOT).

Additionally, we evaluate 3D localization precision on KITTI, measured as Euclidean distance (in meters) between estimated 3D positions and ground-truth trajectories. Fig. 6 shows recall and 3D localization error as a function of distance from the camera for *pedestrians* and *cars*. Both 4D-GVT and CAMOT achieve a small localization error – up to 2m in farther camera ranges – which is not surprising, since they are both based on stereo. CIWT localizes objects using a stereo-based bottom-up segmentation method and switches to monocular localization when it cannot associate a 3D segment to a detection. This way, it can track larger objects (*e.g.* cars) farther than 50m at the price of significantly larger localization errors, even in closer ranges. This confirms that stereo-based localization is essential for high 3D localization precision. Pedestrians can be localized in up to 45m camera range. Interestingly, the fine-tuned variant achieves lower recall after 25m range, but still yields higher MOTA due to less false positives (*i.e.* higher precision).

**Runtime Analysis.** With a small number of frame-level proposals (*e.g.*, only cars and pedestrians, 10-20 inputs/frame), the 4D-GVT require less than 1s/frame. Our method can also operate with a large number of frame-level proposals to provide tubes representing *unknown* objects and trade-off between recall/runtime by a varying number of input proposals – 500 proposals/frame result in the run-

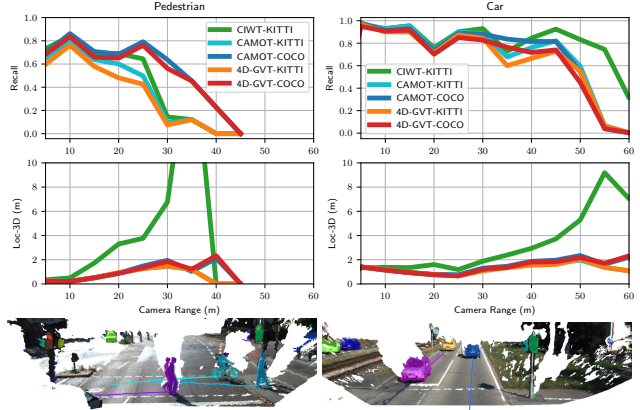


Figure 6: 3D localization evaluation on KITTI MOT for *pedestrian* (left) and *car* (right) class. At the bottom, we show 3D qualitative results.

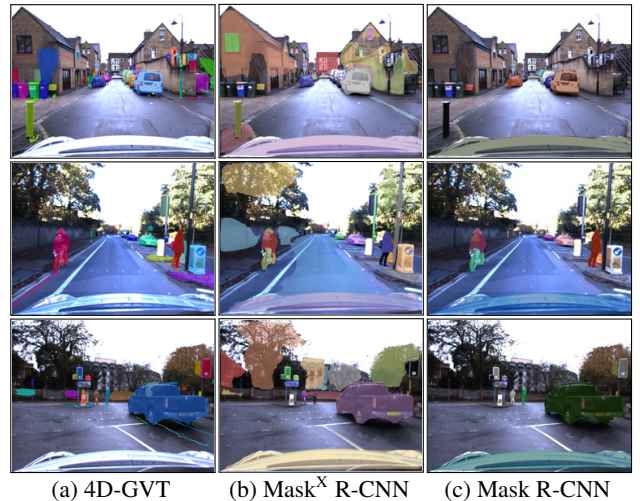


Figure 7: Qualitative comparison of proposed 4D-GVT to Mask R-CNN [15] and Mask<sup>X</sup> R-CNN [21].

time of  $\sim 35$  s/frame. This operation mode is intended for offline processing, *e.g.*, collecting tubes of *unknown* objects. Thus, the proposed method is efficient for extracting tubes for *known* objects only, while it is still suitable for mining arbitrary objects from videos offline.

**Large-Scale Video-Object Mining.** We perform large-scale video object mining using 14h of stereo recordings of the Oxford RobotCar dataset and show a detailed statistics in the supplementary material. In total, we obtained 977,622 video tubes, of which 833,293 (85%) are of an *unknown* class; these represent potentially interesting novel object categories that could be discovered using zero-shot learning techniques.

## 5. Conclusion

In this work we have proposed 4D-GVT for generic video-object tube generation. We have shown that it is indeed possible to precisely localize objects from *known* and

*unknown* categories in 4D space/time, as required by a wide range of robotics and automotive applications. Importantly, we have demonstrated that by combining modern instance segmentation methods with a well-funded tracking framework and using parallax as a consistency filter, 4D-GVT can match the recall of the recent Mask<sup>X</sup> R-CNN method (trained on a significantly larger dataset) while generating high-quality video object tubes as output that precisely localize objects in 3D. We plan to use 4D-GVT as an important building block for unsupervised visual concept discovery from videos and for learning to predict future motion for arbitrary objects.

**Acknowledgments:** This project was funded, in parts, by ERC Consolidator Grant DeeVise (ERC-2017-COG-773161). The experiments were performed with computing resources granted by RWTH Aachen University under project rwth0275.

## References

- [1] A. Alahi, K. Goel, V. Ramanathan, A. Robicquet, L. Fei-Fei, and S. Savarese. Social lstm: Human trajectory prediction in crowded spaces. In *CVPR*, June 2016. 1, 3
- [2] A. Bansal, K. Sikka, G. Sharma, R. Chellappa, and A. Divakaran. Zero-shot object detection. In *ECCV*, 2018. 1, 3
- [3] K. Bernardin and R. Stiefelhagen. Evaluating multiple object tracking performance: The clear mot metrics. *JVIP*, 2008:1:1–1:10, 2008. 7, 12, 13
- [4] W. Brendel and S. Todorovic. Video object segmentation by tracking regions. In *ICCV*, 2009. 1, 2
- [5] W. Choi. Near-online multi-target tracking with aggregated local flow descriptor. In *ICCV*, 2015. 1
- [6] J. Deng, W. Dong, R. Socher, L.-J. Li, K. Li, and L. Fei-Fei. ImageNet: A large-scale hierarchical image database. In *CVPR*, 2009. 12
- [7] A. Dewan, T. Caselitz, G. D. Tipaldi, and W. Burgard. Motion-based detection and tracking in 3d lidar scans. In *ICRA*, 2015. 2
- [8] M. Everingham, L. Van Gool, C. Williams, J. Winn, and A. Zisserman. The pascal visual object classes (VOC) challenge. *IJCV*, 88(2):303–338, 2010. 6
- [9] K. Fragkiadaki, P. A. Arbeláez, P. Felsen, and J. Malik. Learning to segment moving objects in videos. *CVPR*, 2015. 2, 7
- [10] A. Geiger, P. Lenz, and R. Urtasun. Are we ready for autonomous driving? the KITTI vision benchmark suite. In *CVPR*, 2012. 2, 5, 6
- [11] A. Geiger, M. Roser, and R. Urtasun. Efficient large-scale stereo matching. In *ACCV*, 2010. 4
- [12] A. Geiger, J. Ziegler, and C. Stiller. Stereoscan: Dense 3D reconstruction in real-time. In *Intel. Vehicles Symp.*, 2011. 4
- [13] A. Gupta, J. Johnson, L. Fei-Fei, S. Savarese, and A. Alahi. Social gan: Socially acceptable trajectories with generative adversarial networks. In *CVPR*, 2018. 1, 3
- [14] R. Hartley and A. Zisserman. *Multiple view geometry in computer vision*. Cambridge University Press, 2000. 12
- [15] K. He, G. Gkioxari, P. Dollár, and R. Girshick. Mask R-CNN. In *ICCV*, 2017. 1, 2, 3, 5, 6, 8, 12, 13, 16
- [16] K. He, X. Zhang, S. Ren, and J. Sun. Deep residual learning for image recognition. In *CVPR*, 2016. 12
- [17] D. Held, D. Guillory, B. Rebsamen, S. Thrun, and S. Savarese. A probabilistic framework for real-time 3d segmentation using spatial, temporal, and semantic cues. In *RSS*, 2016. 2
- [18] D. Held, J. Levinson, S. Thrun, and S. Savarese. Combining 3d shape, color, and motion for robust anytime tracking. In *RSS*, 2014. 2
- [19] E. Horbert, G. M. Garcia, S. Frintrop, and B. Leibe. Sequence-level object candidates based on saliency for generic object recognition on mobile systems. In *ICRA*, 2015. 2
- [20] R. Hou, C. Chen, and M. Shah. Tube convolutional neural network (t-cnn) for action detection in videos. In *ICCV*, 2017. 1
- [21] R. Hu, P. Dollár, K. He, T. Darrell, and R. Girshick. Learning to Segment Every Thing. In *CVPR*, 2018. 2, 6, 8, 13
- [22] Y. Hu, J. Huang, and A. Schwing. Maskrnn: Instance level video object segmentation. In *NIPS*, 2017. 1, 2
- [23] J. Huang, V. Rathod, C. Sun, M. Zhu, A. Korattikara, A. Fathi, I. Fischer, Z. Wojna, Y. Song, S. Guadarrama, and K. Murphy. Speed/accuracy trade-offs for modern convolutional object detectors. In *CVPR*, 2017. 16
- [24] S. Jin, A. RoyChowdhury, H. Jiang, A. Singh, A. Prasad, D. Chakraborty, and E. Learned-Miller. Unsupervised hard example mining from videos for improved object detection. In *ECCV*, 2018. 2
- [25] D. Klostermann, A. Ošep, J. Stückler, and B. Leibe. Unsupervised learning of shape-motion patterns for objects in urban street scenes. In *BMVC*, 2016. 3
- [26] R. Krishna, Y. Zhu, O. Groth, J. Johnson, K. Hata, J. Kravitz, S. Chen, Y. Kalantidis, L.-J. Li, D. A. Shamma, M. Bernstein, and L. Fei-Fei. Visual genome: Connecting language and vision using crowdsourced dense image annotations. *arXiv preprint arXiv:1602.07332*, 2016. 2, 6
- [27] S. Kwak, M. Cho, I. Laptev, J. Ponce, and C. Schmid. Unsupervised object discovery and tracking in video collections. In *ICCV*, 2015. 1, 2, 3
- [28] N. Lee, W. Choi, P. Vernaza, C. B. Choy, P. H. S. Torr, and M. K. Chandraker. Desire: Distant future prediction in dynamic scenes with interacting agents. *CVPR*, 2017. 1, 3
- [29] Y. J. Lee and K. Grauman. Object-graphs for context-aware visual category discovery. In *CVPR*, 2010. 1, 3
- [30] Y. J. Lee and K. Grauman. Learning the easy things first: Self-paced visual category discovery. In *CVPR*, 2011. 1, 3
- [31] B. Leibe, K. Schindler, N. Cornelis, and L. V. Gool. Coupled object detection and tracking from static cameras and moving vehicles. *PAMI*, 30(10):1683–1698, 2008. 2, 4
- [32] P. Lenz, J. Ziegler, A. Geiger, and M. Roser. Sparse scene flow segmentation for moving object detection in urban environments. In *Intel. Vehicles Symp.*, 2011. 2
- [33] S. Li, B. Seybold, A. Vorobyov, A. Fathi, Q. Huang, and C.-C. J. Kuo. Instance embedding transfer to unsupervised video object segmentation. In *CVPR*, 2018. 2, 7
- [34] T.-Y. Lin, M. Maire, S. Belongie, J. Hays, P. Perona, D. Ramanan, P. Dollár, and C. L. Zitnick. Microsoft COCO: Common objects in context. In *ECCV*, 2014. 2, 5, 6, 7, 12

- [35] W. Lin, Y. Zhou, H. Xu, J. Yan, M. Xu, J. Wu, and Z. Liu. A tube-and-droplet-based approach for representing and analyzing motion trajectories. *PAMI*, 39(8):1489–1503, 2017. **3**
- [36] W. Maddern, G. Pascoe, C. Linegar, and P. Newman. 1 year, 1000km: The Oxford RobotCar dataset. *IJRR*, 36(1):3–15, 2017. **2, 5, 13**
- [37] I. Misra, A. Shrivastava, and M. Hebert. Watch and learn: Semi-supervised learning of object detectors from videos. In *CVPR*, 2015. **2**
- [38] I. Misra, C. L. Zitnick, and M. Hebert. Shuffle and Learn: Unsupervised learning using temporal order verification. In *ECCV*, 2016. **2**
- [39] D. Mitzel and B. Leibe. Taking mobile multi-object tracking to the next level: People, unknown objects, and carried items. In *ECCV*, 2012. **2**
- [40] F. Moosmann and M. Sauerland. Unsupervised discovery of object classes in 3d outdoor scenarios. In *ICCV Workshops*, 2011. **3**
- [41] G. Neuhold, T. Ollmann, S. R. Bulo, and P. Kotschieder. The Mapillary Vistas dataset for semantic understanding of street scenes. In *ICCV*, 2017. **12**
- [42] A. Ošep, A. Hermans, F. Engelmann, D. Klostermann, M. Mathias, and B. Leibe. Multi-scale object candidates for generic object tracking in street scenes. In *ICRA*, 2016. **2**
- [43] A. Ošep, W. Mehner, M. Mathias, and B. Leibe. Combined image- and world-space tracking in traffic scenes. In *ICRA*, 2017. **7**
- [44] A. Ošep, W. Mehner, P. Voigtlaender, and B. Leibe. Track, then decide: Category-agnostic vision-based multi-object tracking. *ICRA*, 2018. **2, 4, 7**
- [45] D. P. Papadopoulos, J. R. R. Uijlings, F. Keller, and V. Ferrari. Extreme clicking for efficient object annotation. In *ICCV*, 2017. **12**
- [46] T. Pham, V. B. G. Kumar, T.-T. Do, G. Carneiro, and I. Reid. Bayesian semantic instance segmentation in open set world. In *ECCV*, September 2018. **3, 6**
- [47] P. Pinheiro, R. Collobert, and P. Dollár. Learning to segment object candidates. In *NIPS*, 2015. **6, 7, 14**
- [48] P. Pinheiro, T. Lin, R. Collobert, and P. Dollár. Learning to refine object segments. In *ECCV*, 2016. **6, 13**
- [49] A. Prest, C. Leistner, J. Civera, C. Schmid, and V. Ferrari. Learning object class detectors from weakly annotated video. In *CVPR*, 2012. **2, 3**
- [50] S. Rahman, S. H. Khan, and F. Porikli. Zero-shot object detection: Learning to simultaneously recognize and localize novel concepts. *ACCV*, 2018. **1, 3**
- [51] D. B. Reid. An algorithm for tracking multiple targets. *IEEE Trans. Automatic Control*, 24(6):843–854, 1979. **2, 3, 4**
- [52] M. Rubinstein, A. Joulin, J. Kopf, and C. Liu. Unsupervised joint object discovery and segmentation in internet images. In *CVPR*, 2013. **1, 3**
- [53] B. C. Russell, W. T. Freeman, A. A. Efros, J. Sivic, and A. Zisserman. Using multiple segmentations to discover objects and their extent in image collections. In *CVPR*, 2006. **1, 3**
- [54] K. Schindler, J. U., and H. Wang. Perspective N-view multibody structure-and-motion through model selection. In *ECCV*, 2006. **5**
- [55] G. Seguin, P. Bojanowski, R. Lajugie, and I. Laptev. Instance-level video segmentation from object tracks. In *CVPR*, 2016. **1**
- [56] J. Sivic, B. C. Russell, A. Zisserman, W. T. Freeman, and A. A. Efros. Unsupervised discovery of visual object class hierarchies. In *CVPR*, 2008. **1, 3**
- [57] D. Stutz and A. Geiger. Learning 3d shape completion from laser scan data with weak supervision. In *CVPR*, 2018. **1, 3**
- [58] K. Tang, V. Ramanathan, L. Fei-fei, and D. Koller. Shifting weights: Adapting object detectors from image to video. In *NIPS*, 2012. **2**
- [59] A. Teichman, J. Levinson, and S. Thrun. Towards 3D object recognition via classification of arbitrary object tracks. In *ICRA*, 2011. **2**
- [60] A. Teichman and S. Thrun. Tracking-based semi-supervised learning. *IJRR*, 31(7):804–818, 2012. **2**
- [61] P. Tokmakov, K. Alahari, and C. Schmid. Learning video object segmentation with visual memory. In *ICCV*, 2017. **2, 7**
- [62] P. Tokmakov, C. Schmid, and K. Alahari. Learning to segment moving objects. *IJCV*, 127:282–301, 2018. **2**
- [63] Y.-H. Tsai, G. Zhong, and M.-H. Yang. Semantic co-segmentation in videos. In *ECCV*, 2016. **3**
- [64] T. Tuytelaars, C. H. Lampert, M. B. Blaschko, and W. Buntine. Unsupervised object discovery: A comparison. *IJCV*, 88:284–302, 2010. **1, 3**
- [65] C. Vogel, K. Schindler, and S. Roth. Piecewise rigid scene flow. In *ICCV*, 2013. **2**
- [66] P. Voigtlaender, M. Krause, A. Ošep, J. Luiten, B. B. G. Sekar, A. Geiger, and B. Leibe. MOTs: Multi-object tracking and segmentation. *arXiv preprint arXiv:1902.03604*, 2019. **12**
- [67] P. Voigtlaender and B. Leibe. Online adaptation of convolutional neural networks for video object segmentation. In *BMVC*, 2017. **1, 2**
- [68] C. Vondrick, A. Shrivastava, A. Fathi, S. Guadarrama, and K. Murphy. Tracking emerges by colorizing videos. In *ECCV*, September 2018. **2**
- [69] L. Wang, G. Hua, R. Sukthankar, J. Xue, Z. Niu, and N. Zheng. Video object discovery and co-segmentation with extremely weak supervision. *PAMI*, 39:2074–2088, 2014. **1, 3**
- [70] X. Wang, M. Yang, S. Zhu, and Y. Lin. Regionlets for generic object detection. In *ICCV*, 2013. **7**
- [71] Y. Wu et al. Tensorpack. <https://github.com/tensorpack/>, 2016. **12**
- [72] Y. Xian, C. H. Lampert, B. Schiele, and Z. Akata. Zero-shot learning - a comprehensive evaluation of the good, the bad and the ugly. *PAMI*, 2018. **1, 3**
- [73] J. H. Yoon, C.-R. Lee, M.-H. Yang, and K.-J. Yoon. Online multi-object tracking via structural constraint event aggregation. In *CVPR*, 2016. **1**
- [74] W. Yuan, T. Khot, D. Held, C. Mertz, and M. Hebert. Pcn: Point completion network. In *3DV*, 2018. **1, 3**

- [75] L. Zhang, L. Yuan, and R. Nevatia. Global data association for multi-object tracking using network flows. In *CVPR*, 2008. [2](#)
- [76] G. Zhu, F. Porikli, and H. Li. Model-free multiple object tracking with shared proposals. In *ACCV*, 2016. [2](#)
- [77] J.-Y. Zhu, J. Wu, Y. Wei, E. Chang, and Z. Tu. Unsupervised object class discovery via saliency-guided multiple class learning. In *CVPR*, 2012. [1, 3](#)
- [78] P. Zhu, H. Wang, and V. Saligrama. Zero shot detection. *IEEE Trans. on Circ. and Systems for Video Tech.*, pages 1–1, 2019. [1, 3](#)

# Supplemental Material

## A. Implementation Details

### A.1. MP R-CNN

MP R-CNN is based on a modified version of a Mask R-CNN [15] network implementation by [71] with a ResNet101 [16] backbone. We adjust this network to be category agnostic by replacing the  $N$  classes with just one class by mapping all classes to a single foreground class for detecting generic objects. Next, we add an additional classification head to the network, so that the network can recover the classification information for each object. We train this network starting from pre-trained ImageNet [6] weights on the COCO dataset [34]. The batch size is one image per GPU that is resized (without changing the aspect ratio) such that the smaller image dimension is 800 if the resulting larger image dimension is no more than 1333. Otherwise, it is resized such that the larger image dimension is 1333 pixels. For optimization, we use the Momentum Optimizer of Tensorflow with an initial learning rate of  $3 \times 10^{-3}$ , a momentum of 0.9 and a learning rate decay schedule as given by [71]. We train this network for 854,100 steps using four TITAN X Pascal GPUs. For data augmentation, we adopt horizontal flipping. Furthermore, we perform non-maximum suppression to remove proposals which have an IoU of 80% or greater with a higher scoring proposal. However, we do not threshold by the score.

### A.2. 4D-GVT

**Ground Plane Estimation.** For video-tubes estimation, we utilize coarse geometric scene knowledge by estimating a ground plane. To perform the ground plane estimation, we 1) use the knowledge about the camera height in order to trim-down the point-cloud, 2) estimate the ground plane with the RANSAC algorithm and iii) refine the estimate of the RANSAC inliers using linear least squares.

**Kalman Filter.** We leverage linear constant-velocity to estimate the 3D position and size of the video tube. Also, we use a Kalman filter for the 3D segment-to-tube association and tube scoring. Based on the 3D localization of the per-frame object proposals in a 3D point cloud, we can robustly compute a median 3D position estimate of the segment and an estimate of the 3D bounding box as explained in the paper. Our approach uses the  $x$  and  $z$  coordinates directly and obtains the observed  $y$ -coordinate estimate by projecting the estimated 3D median position to the ground. Thus, we obtain a projection of the 3D position to the estimated ground plane. This has proven to be very robust to partial occlusions. Similarly, we project the 3D velocity estimate to the ground. In the case that the 3D velocity of a segment was not estimated reliably (e.g. the object is

not well-textured to obtain feature matches), we update the state using only partial observations of the state (3D position and the 3D size estimates). Assuming constant pixel and disparity noise, we obtain the uncertainty in 3D localization and velocity as the uncertainty estimate of the stereo depth estimate using forward error propagation [14].

**Hyperparameter Learning.** All hyperparameters for tube generation, scoring, and co-selection are learned on the KITTI dataset using *car* and *pedestrian* categories, optimized for the MOTA score [3]. In particular, we use sequences 1, 2, 3, 4, 9, 11, 12, 15, 17, 19 and 20 to perform model validation and the rest for the evaluation. For the video-object mining, we manually lower the CRF model parameter  $\epsilon_1$  in order to allow tubes representing *unknown* object categories to be selected as well and assign equal weights (0.33) to  $w_1, w_2$  and  $w_3$ , i.e., to all three terms that contribute to the tube score. Hyperparameter learning would assign a significantly higher weight to the objectness term (weight  $w_3$ ) since in KITTI only *known* objects are evaluated, i.e., the *car*, and *pedestrian* categories.

### A.3. KITTI Fine-tuning of Mask R-CNN

In order to evaluate a KITTI fine-tuned version of Mask R-CNN (the results marked with (KITTI) in Table 4 of the main paper), we use the detections of TrackR-CNN [66]. TrackR-CNN extends Mask R-CNN by 3D convolutions in order to incorporate temporal context. It is pre-trained on COCO [34] and Mapillary [41] and fine-tuned on novel pixel-wise annotations for the KITTI tracking training set.

## B. Additional Experimental Evaluation

### B.1. Oxford RobotCar Labels

In this section, we provide additional details on the Oxford RobotCar labels, which we only used for the recall evaluation. We did not use these labels for training or tuned any hyperparameters using these labels. For the labeling process, we manually selected 150 images which are not too close to each other in time. We labeled 1,494 (1,081 *known*, 413 *unknown*) bounding boxes covering the visible portions of objects (non-amodal) by clicking the extremal points [45]. Examples of labeled objects are shown in Fig. 8. Labeled categories that overlap with the COCO [34] category set are *car*, *person*, *bike* and *bus*. In addition, we labeled several object classes that are not present in the COCO dataset as “other” (pink color). Most notable object classes in the *unknown* set are the following: *signage*, *pole*, *stone road sign*, *traffic cone*, *street sign*, *rubbish bin*, *transformer*, *post box*, *booth*, *stroller*.



Figure 8: Examples of labeled images from Oxford RobotCar [36] dataset. The *unknown* object classes are assigned label “other” (pink color).

Evaluation Criteria	Box Proposals			Segmentation Proposals		
	AR @ 10	AR @ 100	AR @ 1000	AR @ 10	AR @ 100	AR @ 1000
Known COCO Categories (20)	0.421	0.587	0.641	0.348	0.468	0.511
Unknown COCO Categories (60)	0.069	0.179	0.338	0.053	0.134	0.241

Table 4: We evaluate our per-frame poposal generator on *known* and *unknown* categories separately. The trend indicates that the generator is able to generalize to unseen object categories given a sufficient number of proposals, while it performs reasonable on seen object categories. Remark: Since the ground-truth is different (*known* and *unknown*), the numbers are not directly comparable, but the trend is clear.

## B.2. Extended COCO Average Recall Evaluation

### B.3. Image-Level Proposal and Video Tubes Evaluation

Due to lack of space, we omitted a detailed presentation of the recall evaluation in the main paper. Table 6 present a detailed recall evaluation for per-frame object proposals and video tubes (4D-GVT). Specifically, we present the precise recall we obtain for the top-50, 100, 150, 200, and 700 per-frame proposals and video tubes. As in the main paper, **mrcnn-original** refers to vanilla Mask R-CNN [15], **SharpMask** refers to [48], **mxrcnn** refers to Mask<sup>X</sup> R-CNN [21] and finally, **mp-rcnn** refer to our proposed MP R-CNN.

### B.4. Extended CLEAR-MOT Tracking Evaluation

In the main paper, presented only MOTA scores and number of ID switches in the KITTI MOT evaluation tables and omitted the less commonly used MOTP, Mostly-Tracked (MT), Mostly-Lost (ML), Partially-Lost (PT) and Fragments metrics [3]. For completeness, we show all tracking metrics evaluated on the KITTI benchmark in Table 7).

## B.5. Video-Mining Evaluation

Table 8 shows statistics of the tracks we obtained by mining 14h of the Oxford RobotCar dataset. In total, we obtained 977, 622 tracks, of which 833, 293 are of an *unknown* class. This number is significantly larger than the number of tracks for the most common classes such as *person* and *car*. 501 tracks are classified as COCO categories which are very unlikely to occur in the RobotCar dataset (*e.g. elephant*) and most likely stem from classification errors. The average length of our tracks is 18.3 time frames.

## B.6. Additional Qualitative Results

Fig. 9 shows additional qualitative results (a) of our method, (b) Mask R-CNN [15], (c) and (d) of Mask<sup>X</sup> R-CNN [21] with and without score-based thresholding on the Oxford RobotCar dataset. We use the original threshold as provided by [21].

In Fig. 11, we show additional qualitative results on KITTI, highlighting several part of our pipeline. In particular, we show all tubes (column 1 and 2) as 2D and 3D bounding boxes and results after co-selection, where tracked objects are visualized as masks (column 3). These results show that our tubes are well-localized not only in image domain, but in 3D space at 3D bounding box level

Model	Box Proposals			Segmentation Proposal		
	AR @ 10	AR @ 100	AR @ 1000	AR @ 10	AR @ 100	AR @ 1000
DeepMask20	0.139	0.286	0.431	0.109	0.215	0.314
DeepMask20*	0.152	0.306	0.432	0.123	0.233	0.314
MP R-CNN20	0.261	0.412	0.517	0.223	0.321	0.390
MP R-CNN80	0.421	0.608	0.662	0.355	0.494	0.539

Table 5: Following the evaluation protocol of DeepMask [47], we show the generalization capabilities of our proposal generator on image-level by training on 20 COCO categories and evaluating on all 80 COCO categories.

	50	100	150	200	700		50	100	150	200	700
mp-rcnn	0.93	0.95	0.95	0.96	0.96	mp-rcnn	0.16	0.28	0.38	0.44	0.72
m-rcnn-original	0.94	0.95	0.95	0.96	0.96	m-rcnn-original	0.14	0.24	0.33	0.38	0.61
mx-rcnn	0.79	0.84	0.84	0.84	0.84	mx-rcnn	0.47	0.58	0.58	0.58	0.58
sharpmask	0.72	0.78	0.79	0.80	0.85	sharpmask	0.28	0.35	0.37	0.41	0.47
4D-GVT-all	0.69	0.80	0.84	0.86	0.90	4D-GVT-coselect	0.42	0.55	0.60	0.63	0.63
4D-GVT-coselect	0.76	0.84	0.87	0.87	0.87	4D-GVT-all	0.31	0.43	0.50	0.54	0.66
CAMOT	0.81	0.81	0.81	0.81	0.81	CAMOT	0.41	0.41	0.41	0.41	0.41

Table 6: Image-level and video tube (dashed) proposal and video-tube recall evaluation (Oxford RobotCar, left: *known*, right: *unknown*). This table supplements Fig. 4 in the main paper.

as well. In addition, this results highlights the effect of co-selection.

Finally, we perform an additional experiment, where we use Mask<sup>X</sup> R-CNN for 4D-GVT instead of MP-RCNN, and show results in Fig. 12. We highlight exactly the same parts of the pipeline as in Fig. 11 and obtain excellent results. We believe that the combination of large-scale training of frame-level proposals in combination with 4D-GVT shows a great promise for future video-object mining and generic object tracking.

	MOTA	MOTP	MT	ML	IDS	Recall	Fragments	Precision
CIWT (KITTI)	0.33	0.71	0.54	0.10	42	0.69	123	0.67
4D-GVT (KITTI)	0.33	0.68	0.34	0.15	18	0.59	157	0.70
CAMOT (KITTI)	0.26	0.68	0.34	0.09	72	0.63	224	0.65
4D-GVT (COCO)	0.27	0.71	0.53	0.10	24	0.71	138	0.62
CAMOT (COCO)	-0.05	0.71	0.57	0.03	214	0.74	321	0.51

(a) Car.

	MOTA	MOTP	MT	ML	IDS	Recall	Fragments	Precision
CIWT (KITTI)	0.65	0.79	0.62	0.05	8	0.82	82	0.84
4D-GVT (KITTI)	0.61	0.81	0.53	0.14	6	0.73	46	0.88
CAMOT (KITTI)	0.60	0.81	0.52	0.09	40	0.73	92	0.88
4D-GVT (COCO)	0.57	0.82	0.51	0.20	4	0.70	34	0.86
CAMOT (COCO)	0.54	0.81	0.51	0.09	174	0.74	237	0.84

(b) Pedestrian.

Table 7: CLEAR-MOT evaluation on KITTI MOT dataset. This is an extended version of Tab. 3 in the main paper.

Category	#Tracks	Avg. Track Length (Frames)	Median Track Length (Frames)
<i>person</i>	59,605		24.0
<i>car</i>	49,227		33.1
<i>bicycle</i>	17,324		21.7
<i>traffic light</i>	5,802		60.1
<i>truck</i>	2,255		44.8
<i>motorcycle</i>	2,063		24.8
<i>handbag</i>	2,013		14.1
<i>bus</i>	1,591		46.2
<i>bench</i>	867		23.3
<i>backpack</i>	813		16.8
<i>potted plant</i>	666		28.6
<i>umbrella</i>	565		17.5
<i>stop sign</i>	269		51.6
<i>chair</i>	263		20.3
<i>suitcase</i>	160		22.6
<i>fire hydrant</i>	147		22.4
<i>parking meter</i>	99		31.1
<i>train</i>	70		15.5
<i>dog</i>	27		20.2
<i>cat</i>	2		6.0
<i>unknown</i>	833,293		16.5
<i>other COCO</i>	501		20.5
Total	977,622		18.3

Table 8: Statistics for mining 14h of Oxford data. Other COCO are categories which are unlikely to occur in outdoor street scenes (probably classification errors).



Figure 9: Qualitative comparison of our proposed (a) 4D-GVT, (b) Mask R-CNN [15], (c) Mask<sup>X</sup> R-CNN [23]; (d) additionally visualizes all Mask<sup>X</sup> R-CNN instance segmentations (non-thresholded using the recommended settings) on the Oxford RobotCar dataset. As can be seen, our approach generates a better interpretation for the relevant street scene objects, while producing fewer clutter proposals overall.



Figure 10: Additional qualitative results on KITTI, visualized as 3D point clouds. Here we show only high-scoring tubes.



(a) 2D boxes (all)

(b) 3D boxes (all)

(c) Masks (co-selection)

Figure 11: Additional qualitative results of 4D-GVT using MP R-CNN proposals as frame-level inputs. We show all tubes (as 2D and 3D bounding boxes) and results obtained after the co-selection (shown as masks).



Figure 12: As an additional experiment, we used Mask<sup>X</sup> R-CNN as frame-level inputs for 4D-GVT (all outputs from the network, not only the confident ones). We show all tubes (as 2D and 3D bounding boxes) and results obtained after the co-selection (shown as masks).